Design, synthesis and in vitro and in vivo antitumour activity of 3-benzylideneindolin-2-one derivatives, a novel class of small-molecule inhibitors of the MDM2–p53 interaction

ARTICLE *in* EUROPEAN JOURNAL OF MEDICINAL CHEMISTRY · JANUARY 2014

Impact Factor: 3.45

8 AUTHORS, INCLUDING:

Zhen Wang
Beijing Technology and Business University
121 PUBLICATIONS **1,108** CITATIONS
SEE PROFILE

Xing-yue Ji
Peking Union Medical University
8 PUBLICATIONS **21** CITATIONS
SEE PROFILE

Zhuo-Rong Li
52 PUBLICATIONS **590** CITATIONS
SEE PROFILE

European Journal of Medicinal Chemistry 81 (2014) 277–288

Contents lists available at ScienceDirect

European Journal of Medicinal Chemistry

journal homepage: http://www.elsevier.com/locate/ejmech

Original article

Design, synthesis and *in vitro* and *in vivo* antitumour activity of 3-benzylideneindolin-2-one derivatives, a novel class of small-molecule inhibitors of the MDM2–p53 interaction

Guang-hui Zheng, Jia-jia Shen, Yue-chen Zhan, Hong Yi, Si-tu Xue, Zhen Wang, Xing-yue Ji*, Zhuo-rong Li*

Institute of Medicinal Biotechnology, Chinese Academy of Medical Science and Peking Union Medical College, Beijing 100050, People's Republic of China

ARTICLE INFO

Article history:
Received 4 November 2013
Received in revised form
5 May 2014
Accepted 6 May 2014
Available online 9 May 2014

Keywords:
Small-molecule inhibitors
MDM2–p53 interaction
Antiproliferative activity

ABSTRACT

A novel class of small-molecule inhibitors of MDM2–p53 interaction with a (*E*)-3-benzylideneindolin-2-one scaffold was identified using an integrated virtual screening strategy that combined both pharmacophore- and structure-based approaches. The hit optimisation identified several compounds with more potent activity than the hit compound and the positive drug nutlin-3a, especially compound **1b**, which exhibited both the highest binding affinity to MDM2 (K_i = 0.093 μM) and the most potent antiproliferative activity against HCT116 (wild type p53) cells (GI_{50} = 13.42 μM). Additionally, **1b** dose-dependently inhibited tumour growth in BALB/c mice bearing CT26 colon carcinoma, with no visible sign of toxicity. In summary, compound **1b** represents a novel and promising lead structure for the development of anticancer drugs as MDM2–p53 interaction disruptors.

1. Introduction

The tumour suppressor protein p53 plays a pivotal role in DNA repair, cell cycle regulation and apoptosis [1,2]. Moreover, this protein is an attractive anticancer therapeutic target because it can be functionally activated to eradicate tumour. It has been established that the p53 protein is mutated or deleted in half of human cancers. In the remaining cases, p53 retains its wild type form, but its activity is inhibited by the human murine double minute 2 (MDM2, also known as HDM2) oncoprotein via the following mechanisms: a) binding to the p53 transactivation domain to inhibit its transcriptional activity, b) exporting p53 out of the nucleus, and c) promoting proteasome-mediated degradation of p53 [3]. Consequently, blocking the MDM2–p53 interaction to reactivate p53 is a promising anticancer therapeutic strategy.

One successful approach for targeting protein–protein interactions (PPIs) is the rational design of small-molecules that mimic the interaction of a few key residues (i.e., hot spots) at the protein–protein interface [4]. Unlike common PPIs, in which the interface is large, shallow and nondescript [5], the MDM2-p53 interface consists of a cluster of narrow and deep hydrophobic clefts that could be targeted by small-molecule inhibitors. Mutational analysis and alanine scanning of p53 peptides revealed that the Phe19, Trp23 and Leu26 residues (hot spots) play an important role in the interaction between p53 and MDM2 (Fig. 1) [6]. Hence, these residues could be used as a template to design small-molecule inhibitors. To date, there are over 20 different chemotypes that have been shown to antagonise the MDM2–p53 interaction, including nutlins [7], benzodiazepinediones [8], isoindolinones [9], chalcones [10], piperidinones [11], pyrrolidones [12], pyrrolopyrimidines [13], spiro-oxindoles [14], and chromenotriazolopyrimidine [15], xanthones [16]. Among these, the nutlins, spiro-oxindoles (MI derivatives), and piperidinones (AM-8553) have shown the most potential for development as clinical agents to treat cancer (Fig. 1). Although these compounds share different scaffold structures, they all inhibit the MDM2–p53 interaction by mimicking the three hot spots residues of p53 (Fig. 1).

The nutlins were identified as the first class of potent, non-peptide, specific inhibitors of the MDM2–p53 interaction by high throughput screening [7]. One of nutlin derivatives, nutlin-3a, binds with high affinity to MDM2, and it is orally active with no visible sign of toxicity in mouse models of human cancer containing wild-type p53 [7,17]. One nutlin derivative, RO5045337, has already entered phase I clinical trials [18]. Using a computational structure-based *de novo* design strategy, Wang's group discovered a new class of inhibitors of the MDM2–p53 interaction, spiro-oxindoles [14].

* Corresponding authors.
E-mail addresses: jixingyue@imb.pumc.edu.cn (X.-y. Ji), l-z-r@263.net (Z.-r. Li).

http://dx.doi.org/10.1016/j.ejmech.2014.05.027

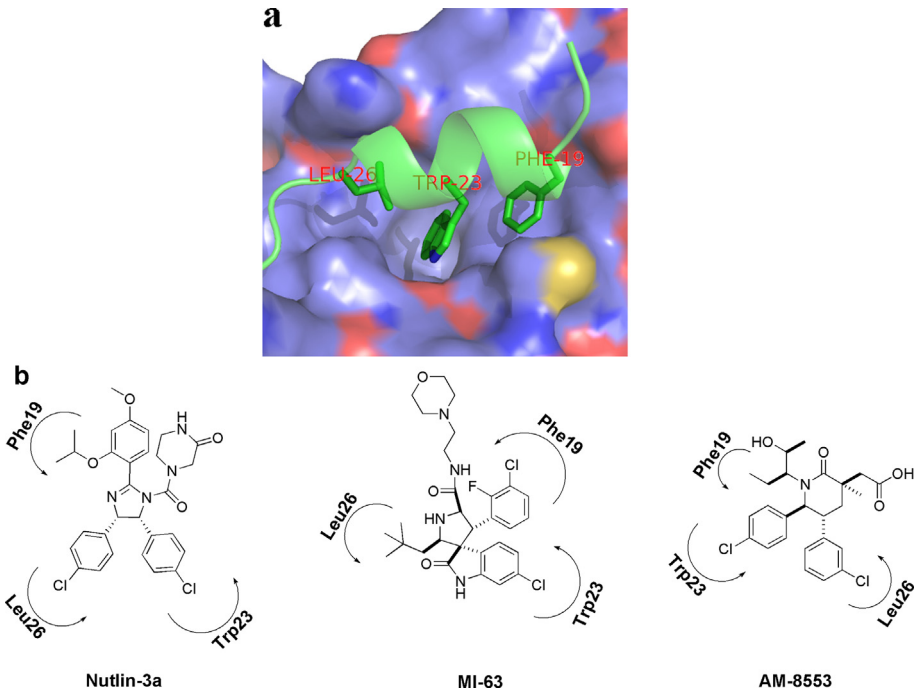

Fig. 1. a: The three hot spots residues involved in the MDM2–p53 interaction (PDB ID: 1YCR; the figure was generated using PyMol). b: The chemical structures of three main inhibitors of the MDM2–p53 interaction and their modes of binding to MDM2.

Further optimisation lead to the compound MI-219, which has potent inhibitory activity (K_i = 13.2 nM) and superior pharmacokinetics (PK) profiles (oral bioavailability F = 65%) [19]. Compound MI-773, which was derived from this scaffold, has also entered phase I clinical trials [18]. Recently, another promising inhibitor, AM-8553, containing a piperidinone scaffold was designed using a structure-based *de novo* strategy. This compound was reported to have potent activity both *in vitro* and *vivo*, along with an oral bioavailability of 100% in rats [11].

In summary, the interaction between MDM2 and p53 represents a promising target for the development of novel anticancer drugs that could be targeted by small-molecule inhibitors. To date, although over 20 small-molecule inhibitors with a diversity array scaffolds have been discovered, around 6 candidate compounds with potent inhibitory activity and superior PK profiles have entered clinical development [18]. It would therefore be highly desirable to discover a novel small-molecule inhibitor with potent activity and an improved ADMET profile.

In this study, we sought to discover novel small-molecule inhibitors of the MDM2–p53 interaction with potent affinity. We identified a novel class of MDM2-p53 inhibitors with a 3-benzylidene-indolin-2-one scaffold by combining both pharmacophore- and structure-based methods as a virtual screening strategy. Hit optimisation was also conducted, and the preliminary structure–activity relationships were assessed. Additionally, a compound with relatively potent activity *in vitro* was chosen to further assay its antitumour activity *in vivo*.

2. Results and discussion

2.1. Virtual screening and hit identification

Computer-aided drug design (CADD) plays an indispensable role both in the discovery and optimisation of hit/lead compounds. Currently, two computational 3D database-screening approaches are available, pharmacophore- and structure-based approaches. The primary advantages of the pharmacophore-based method are its high screening speed and rapid elimination of compounds without critical binding elements. However, this method suffers from a high false positive rate because it does not consider the receptor. Alternatively, the structure-based method (docking) can quantitatively assess the binding affinity of a compound for its target protein, but this process is rather time-consuming. Clearly, these two methods complement each other in terms of screening speed and accuracy of screening results; hence, combining these two complementary approaches is a valid screening strategy [20,21].

In this study, we employed an integrated screening strategy combining pharmacophore- and structure-based methods. It is widely accepted that the interaction between inhibitors and MDM2 primarily involve three hydrophobic pockets (Phe19, Trp23 and Leu26). Based on this information, a simple pharmacophore model was constructed manually in Discovery studio 3.0 (DS 3.0). First, the crystal structure of a known inhibitor (Pip-1, a derivative of the piperidinones) complexed with MDM2 (PDB ID: 2LZG) was employed as reference, and four hydrophobic features (Fig. 2, blue (in the web version) spheres) were constructed manually based on its interaction with MDM2. Additionally, to avoid receptor interactions, the α-C atoms of the amino acids within 5 Å of the ligand were selected and marked as exclusion volumes (Fig. 2, grey spheres).

To validate the generated pharmacophore hypotheses, a test set consisting of 16 active compounds and 48 inactive compounds was collected. The active compounds were all extracted from the PDB database and the reported literature, and the inactive compounds, also known as the decoy set, were derived according to Wallach's method [22]. The compounds in the decoy set had to satisfy the following constraints with respect to the reference drug (Pip-1): a) molecular weight of ±40 Da; b) the exact same number of rotational bonds, hydrogen bond donors (HBDs), and hydrogen bond acceptors (HBAs); c) a CLogP of ±1.0 (ALogP was used here); and d) a Tanimoto coefficient of less than 0.9. The "Screen library" and

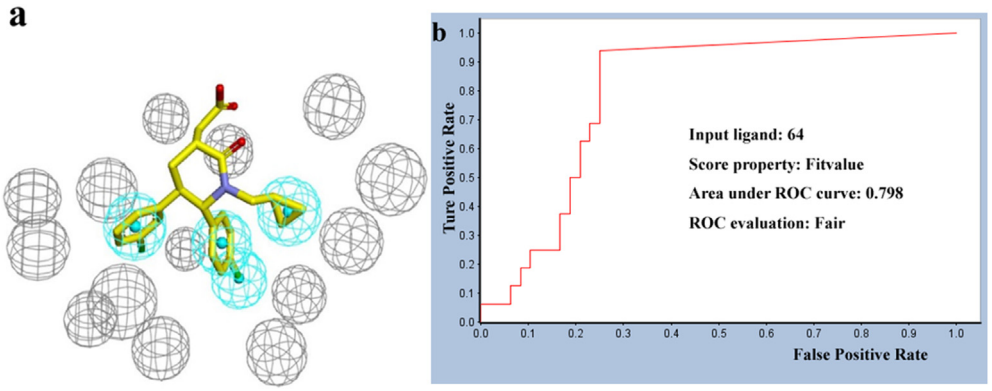

Fig. 2. a: The manually constructed pharmacophore model with exclusion volumes. b: The ROC curve for the generated pharmacophore.

"Calculate ROC Curve" modules in DS 3.0 were used, and 15 of 16 inhibitors were enriched from the test set; however, 12 non-inhibitors were also retrieved (false positives). The area under the ROC curve was 0.798, and the ROC evaluation was "fair". These results indicate that this pharmacophore was sufficiently good to be used as a 3D query to retrieve potential hit compounds.

The validated pharmacophore hypothesis was then used as a 3D query for retrieving potential inhibitors from S406-SETA, S406-SETB, Maybridge and the NCI database in Catalyst. The "Screen library" module in DS 3.0 was used. The "Conformation generation" was set to "fast", and the other parameters were set as default. The identified compounds were further filtered by the Lipinski's rule of five. Lastly, a total of approximately 6000 compounds were retrieved for further docking studies (structure-based approach).

2.2. Docking study and biological assay in vitro

To further verify the compounds identified by pharmacophore mapping, the 6000 retrieved compounds were docked into the p53 binding pockets of MDM2. The protein structure PDB ID 3LBL was chosen as the reference receptor because its ligand had high binding affinity (K_i = 32 nM) and high resolution (1.6 Å). Docking was performed using sybyl 7.3, and the Surflex-Dock module (SFXC) was employed. All the parameters were set as default. After docking, the potential hits were cherry-picked for synthesis and biological assays *in vitro* based on their docking scores, scaffold diversity, synthesizability, and most importantly, their docking poses. Based on their docking poses predicted by SFXC, we performed a visual inspection to confirm that all the chosen potential hits mimicked the three hot spot residues of p53 and occupied the three main hydrophobic pockets of MDM2. Ultimately, 10 compounds with diversity of scaffolds (Please refer to Supplementary data) were selected for synthesis, and each was subjected to fluorescence polarisation assay to validate their inhibitory activity against the MDM2–p53 interaction; nutlin-3a, which is one of the most potent inhibitors of the MDM2–p53 interaction, was used as the positive control.

Fortunately, one compound (**4b**, Fig. 3) showed relatively high binding affinity (K_i = 0.23 μM) to MDM2 with (*E*)-3-benzylideneindolin-2-one scaffold, and hence compound **4b** was identified as hit compound for further optimisation.

2.3. Design

To gain a better understanding of the interaction between compound **4b** and MDM2, we proposed a possible binding mode of compound **4b** and MDM2 based on its docking pose generated by Autodock, which is one of the most widely used docking programmes [23]. As shown in Fig. 4, benzene ring A and the propoxyl groups on the 2- and 4-position (**R_3 & R_5**) of benzene ring B occupied the hydrophobic pockets of Phe19, Trp23, and Leu26, respectively. By analysing the binding modes of known inhibitors to MDM2, we concluded that hydrophobic aromatic rings with

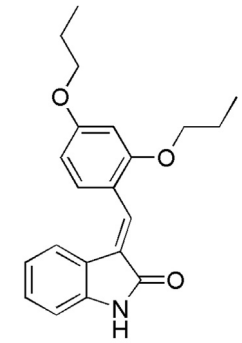

4b: K_i = 0.23 μM

Fig. 3. a: Chemical structure of compound **4b**. b: Inhibitory activity of compound **4b** against the MDM2–p53 interaction in MCF7 cells (co-immunoprecipitation experiment).

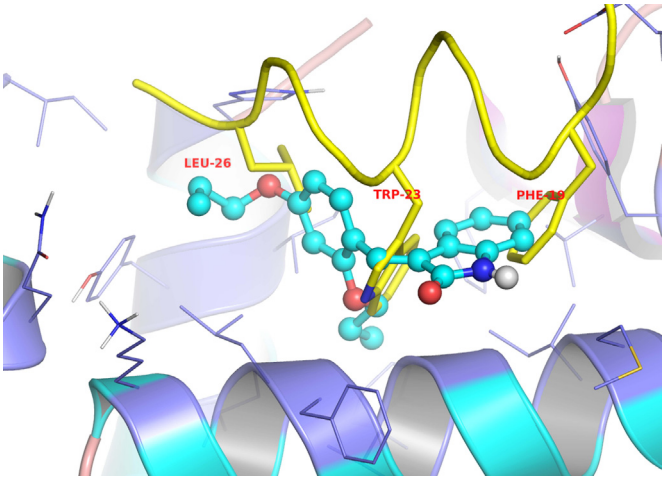

Fig. 4. The proposed binding mode of compound **4b** to MDM2 (generated using PyMol).

halogen substituents favourably occupied the Trp23 pocket. Additionally, given that the biphenyl scaffold is a privileged structure in medicinal chemistry, we designed and synthesised a series of compounds with phenyl substituted at the 2-position **(R_3)** of benzene ring B (**1f**–**3f**, **1h** and **2h**). Given that there were no substituents on the ring A, which likely made it vulnerable to metabolism, compounds with substituents on ring A were synthesised to make them metabolically stable and to investigate the SAR on ring A. Halogens play a vital role in drug development, and around 25% of the "top 200 brand name drugs by retail dollar in 2009" possesses halogens in their chemical structures. Additionally, halogens show a potential ability to form halogen bonding with the target. Consequently, the substituents chosen here were primarily halogens (F and Cl) [24]. In addition, other compounds with various substituents on benzene ring B (**1b**–**7b**) were synthesised to assay their binding affinity to MDM2 using fluorescence polarisation assay.

2.4. Chemistry

As shown in Scheme 1, compound **4b** and several derivatives were synthesised. 2, 4-Dihydroxybenzaldehyde was used as the starting material, and it was used in reactions with alkyl iodide to yield compounds **1a**–**3a**. These compounds were then condensed with substituted indolin-2-one in ethanol under reflux using piperidine as the base to afford the target compounds **1b**–**7b**.

The configuration of the double bond in compounds **1b**–**7b** was assigned to *E* based on the results of the NOESY experiment. In this experiment, a strong interaction between the hydrogen atom at the 4-position of ring A and the 2-position **(R_3)** of ring B was observed, and there was no interaction between the hydrogen atom on the double bond and the hydrogen bond at the 4-position **(R_5)** of ring A (Scheme 1). Additionally, the X-ray single crystal structure of compound **1b** was determined. As shown in Fig. 5, benzene rings A and B were on the same side of the double bond, as expected.

Based on the binding mode of compound **4b** to MDM2, a series of derivatives with substituted phenyl at the 2-position **(R_3)** of benzene ring B were designed and synthesised. As depicted in Scheme 2, substituted bromobenzene was coupled with bis(pinacolato)diboron using tetrakis(triphenylphosphine)palladium as the catalyst to produce compounds **1d** and **2d**. Under the conditions of the Suzuki coupling reaction, compound **2d** was reacted with substituted 2-bromobenzaldehyde to yield compounds **1e** and **2e**, which were further condensed with the substituted indolin-2-one to afford the target compounds **1f**-**3f**. However, when compound

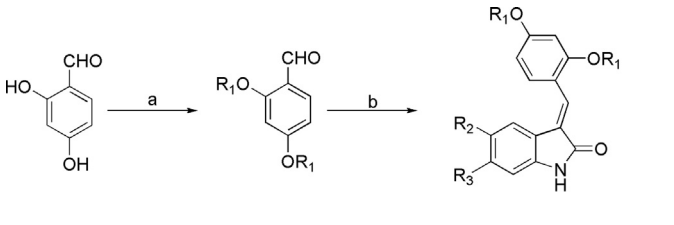

1a: R_1 = Me
2a: R_1 = *n*-Pr
3a: R_1 = *i*-Pr

1b: R_1 = Me, R_2 = R_3 = H
2b: R_1 = Me, R_2 = Cl, R_3 = H
3b: R_1 = Me, R_2 = H, R_3 = F
4b: R_1 = *n*-Pr, R_2 = R_3 = H
5b: R_1 = *n*-Pr, R_2 = Cl, R_3 = H
6b: R_1 = *i*-Pr, R_2 = Cl, R_3 = H
7b: R_1 = *i*-Pr, R_2 = H, R_3 = Cl

Scheme 1. Conditions and reagents: a) K_2CO_3, DMF, alkyl iodide, 60 °C, 80–90%; b) EtOH, piperidine, substituted indolin-2-one, reflux, 4 h, 80–90%.

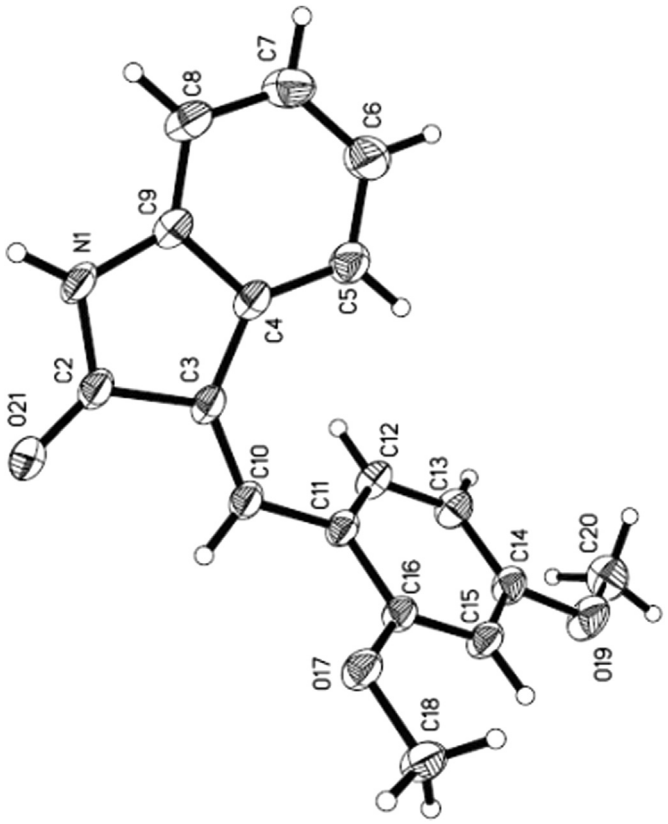

Fig. 5. Scheme of compound **1b** with atom-numbering. The displacement parameters are shown at the 30% probability level.

1d was coupled with the substituted 2-bromobenzaldehyde, no trace of the corresponding target compounds was detected. We therefore adjusted the reaction sequence. The substituted indolin-2-one was first condensed with 2-bromo-4-methoxybenzaldehyde to produce compounds **1g** and **2g**, which were then coupled with compound **1d** under the conditions of the Suzuki coupling reaction to afford the desired compounds. The configuration of the double bond of all the target compounds was confirmed using the NOESY experiment (Scheme 3).

2.5. MDM2 binding affinity and structure activity relationships

The MDM2 binding affinity of all the target compounds was determined by fluorescence polarisation assay. Nutlin-3a was used as positive control to validate our assay, and the results were summarised in Table 1.

As shown in Table 1, our assay was validated by the positive control nutlin-3a, of which the K_i value (0.11 μM) was comparable to the reported one (0.23 μM) [12]. In general, all of the synthesised compounds showed high binding affinity to MDM2, and this was especially true for compounds **1b**, **2b**, **1f**, **2f**, **1h** and **2h**, which exhibited superior or comparable activity to nutlin-3a. Unexpectedly, of all the synthesised compounds, **1b** showed the most potent activity with a K_i value of 0.093 μM. This effect was not consistent with the binding mode of **4b** to MDM2 given that the Trp23 pocket was less occupied in the presence of the methoxyl group compared to its *n*-propoxyl substituted counterpart. The only reasonable explanation is that compound **1b** displayed a distinct binding mode to MDM2. As depicted in Fig. 6, a binding mode of compound **1b** to MDM2 was proposed based on its docking pose generated by Autodock. A hydrogen bond was formed between His-96 of MDM2

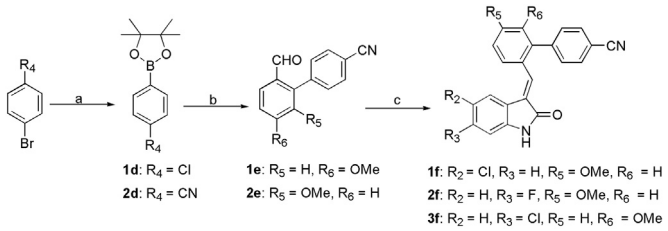

Scheme 2. Conditions and reagents: a) Bis(pinacolato)diboron, KOAc, $Pd(PPh_3)_4$, DMSO, 85 °C, 4 h, N_2, 75%; b) substituted 2-bromobenzaldehyde, Ce_2CO_3, $Pd(PPh_3)_4$, N_2, 120 °C, 4 h, 70–80%; c) EtOH, piperidine, substituted indolin-2-one, reflux, 4 h, 80–90%.

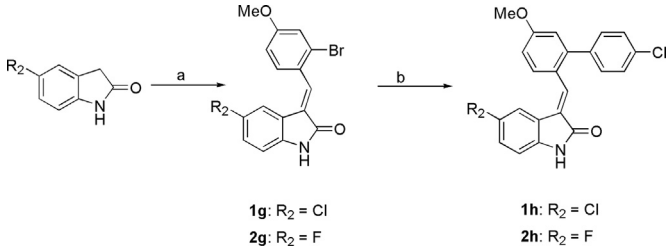

Scheme 3. Conditions and reagents: a) EtOH, piperidine, aldehyde, reflux, 3 h, 80–90%; b) **1d**, Ce_2CO_3, $Pd(PPh_3)_4$, N_2, 120 °C, 4 h, 70–80%.

and the carbonyl group of compound **1b**, and the ring A and B just occupied the Phe19 and Trp23 pocket, respectively. The Leu26 pocket was less occupied.

In terms of the structure–activity relationships, introduction of the chloro group at 5-position **(R_2)** of the indolin-2-one ring (**2b**) had little influence on the binding affinity compared to **1b**. However, decreased inhibitory activity was observed when replacing the H atom at 6-position **(R_1)** of the indolin-2-one (**1b**) with a fluoro group (**3b**). Replacing the methoxyl group at 2-position **(R_3)** of B ring (**2b**) with a bromine atom (**1g**) also slightly decreased the activity. In the case of compound **4b**, both introduction of a chloro substituent at 5 or 6-position **(R_2 & R_1)** and substitution the *iso*-propoxyl group for the *n*-propoxyl group did not alter the binding affinity. When the *n*-propoxyl groups at the 2- and 4-positon **(R_3 & R_5)** of the B ring were replaced by 4-chloro phenyl or 4-cyano phenyl substituents and a methoxyl group, respectively, we observed a slight increase in the binding affinity to MDM2, which was in consistence with the binding mode of compound **4b** to MDM2. Migration of the methoxyl group from 4-position **(R_5)** to 3-position **(R_4)** of ring B (**3f**) showed little influence on the binding affinity.

The binding mode of compound **2h** to MDM2 was also proposed based on its docking pose generated by Autodock. As depicted in Fig. 7, compound **2h** shared a similar binding mode to that of compound **4b**. As expected, the 4-chloro phenyl group occupied the Trp-23 hydrophobic pocket, but the methoxyl group left the Phe-19 pocket less occupied, and this may explain why compounds with substituted phenyl at ring B only showed slight increase in binding affinity compared to their propoxyl substituted counterparts.

2.6. In-vitro antiproliferative activity

The synthesised compounds were further assayed for their antiproliferative activity in human colon cancer (HCT116 with wild type p53), HCT116 (p53 null), lung adenocarcinoma (A549) and breast adenocarcinoma cells (MCF7) cells using MTT assay with 48 h exposure time of the tested compounds, and nutlin-3a was used as positive control. The results were summarised in Table 2.

In general, all of the synthesised compounds showed a certain degree of antiproliferative activity against HCT116 (both wild type p53 and p53 null) cells, and the majority of the target compounds also presented some antiproliferative activity against the A549 and MCF7 cell lines. The difference in cytotoxicity of synthesised compounds between tumour cells with wild type p53 (HCT116, A549, MCF7) may be attributed to: firstly, as the target, the amounts of endogenous MDM2 in three cell lines are different, so the cytotoxicity of selected compounds to the three cancer cell lines varied; secondly, the three cell lines are from different tissues; last but not least, other tumour suppressor genes may be present in A549 and MCF-7, which may lead to reduced activity. Notably, compounds **1b**, **3b**–**7b**, **1f**, **2f**, **1h** and **2h** exhibited superior or comparable activity against HCT116 (p53+/+) to nutlin-3a. In particular, compound **1b** with the most potent inhibitory activity against MDM2–p53 interaction ($K_i = 0.093$ μM) also showed the best inhibitory activity against HCT116 (wild type p53). Additionally, all the tested compounds showed relatively lower GI_{50} values against HCT116 (wild type p53) compared to HCT116 with p53 deleted, demonstrating the selectivity of the synthesised compounds over cancer cell lines with deleted p53. Since compound **1b** showed both the highest binding affinity to MDM2 and the most potent antiproliferative activity, it was chosen for further mechanism study.

2.7. Western blotting analyses

p53 is activated by the inhibition of the MDM2–p53 interaction, resulting in the increased expression of wild-type p53 in cells. Subsequently, p53 activation results in increased levels of p21 and MDM2 [7]. To further verify the anticancer mechanism of this class of compounds, western blotting was used to assess the effects of compound **1b** in HCT116 cells. The cells were treated with compound **1b** or the positive control nutlin-3a for 48 h. Next, the cells were lysed and protein extracts were analysed by western blotting to determine the levels of p53, p21 and MDM2. As shown in Fig. 8, compound **1b** increased the levels of p21, p53 and MDM2 in a dose-dependent manner in HCT116 cells.

2.8. Cell cycle analysis

To gain a better understanding of the mechanisms that underlie the antiproliferative activities of this series of compounds, we investigated the effect of compound **1b** on the cell cycle in HCT116 (wild type p53) cells. HCT116 cells were treated with compounds **1b** and nutlin-3a for 48 h. The fixed cells were stained with propidium iodide (PI) and detected using flow cytometry. As shown in Fig. 9, both compound **1b** and nutlin-3a arrested cells in G2/M phase and induced apoptosis in a dose-dependent manner in HCT116 cells. Moreover, at the same concentrations, compound **1b** induced more apoptosis than nutlin-3a in HCT116 cells.

2.9. In vivo antitumour activity

To further test the therapeutic potential for the synthesised compounds, compound **1b** was chosen to evaluate its antitumour activity in the BALB/c mice bearing colon carcinoma cell line CT26 (CT26 rather than HCT116 cell line was chosen to evaluate the antitumour activity of **1b** preliminarily, and the HCT116 xenograft model will be employed to further investigate the *in-vivo* antitumour activity of **1b** in near future). Before the experiment, the configuration of double bonds of compound **1b** was confirmed again by NOE experiment, and the isomerisation of the double bond was not observed.

Table 1
The MDM2 binding affinity of the synthesised compounds.

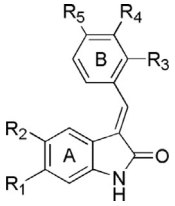

Compounds	R_1	R_2	R_3	R_4	R_5	K_i (μM)[a]
1b[b]	H	H	OMe	H	OMe	0.093
2b[b]	H	Cl	OMe	H	OMe	0.14
1g	H	Cl	Br	H	OMe	0.23
3b	F	H	OMe	H	OMe	0.34
4b	H	H	O-*n*-Pr	H	O-*n*-Pr	0.23
5b	H	Cl	O-*n*-Pr	H	O-*n*-Pr	0.28
6b	H	Cl	O-*i*-Pr	H	O-*i*-Pr	0.24
7b[b]	Cl	H	O-*i*-Pr	H	O-*i*-Pr	0.20
1f	H	Cl	4-CN-Ph	H	OMe	0.15
2f[b]	F	H	4-CN-Ph	H	OMe	0.14
3f	Cl	H	4-CN-Ph	OMe	H	0.19
1h	H	Cl	4-Cl-Ph	H	OMe	0.14
2h	H	F	4-Cl-Ph	H	OMe	0.10
Nutlin-3a	–	–	–	–	–	0.11

[a] K_i values were determined by fluorescence polarisation assay.
[b] These compounds were tested as a mixture of isomers, and the ratio of the *Z* isomers is less than 5% (Please refer to Supplementary data).

First, compound **1b** was dissolved in 10% DMSO and administered via an intraperitoneal injection to two groups of BALB/c mice (10 mice for each group) at doses of 500 mg/kg and 1000 mg/kg, respectively, to determine the maximum administration dosage. No death or visible side effects were observed in the 500 mg/kg dosage group over 8 days. However, all of the mice died within 24 h after the injection of 1000 mg/kg compound **1b**. Therefore, the doses used to evaluate the efficacy of compound **1b** were initially set at 50 mg/kg and 100 mg/kg, and oxaliplatin (1.5 mg/kg) was used as the positive control.

CT26 cancer cell suspensions were implanted subcutaneously into the right axilla region of the mice, and all the mice were divided randomly into the following 5 groups (10 mice/group): compound **1b** (50 mg/kg and 100 mg/kg), oxaliplatin (1.5 mg/kg), vehicle and control groups. The BALB/c mice bearing CT26 colon carcinoma were treated with compound **1b** (100 and 50 mg/kg), oxaliplatin (1.5 mg/kg) or the vehicle via an intraperitoneal injection, and the each treatment was given once daily for 10 days. At the end of the study, all of the mice were weighed and sacrificed, and the tumours were excised and weighed for analysis. The ratio of tumour growth inhibition was calculated using the following formula: $(A - B)/A \times 100\%$ (where A is the average tumour weight of the control group, and B is the average tumour weight of the experimental group). The results were summarised in Table 3.

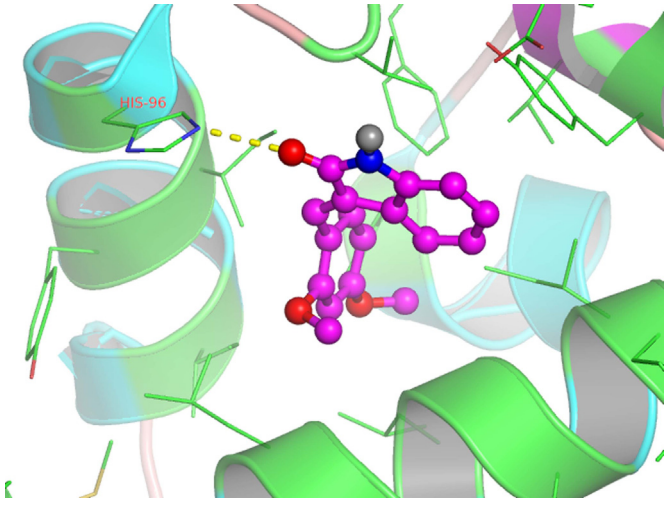

Fig. 6. Proposed binding mode of compound **1b** to MDM2 (generated using PyMol).

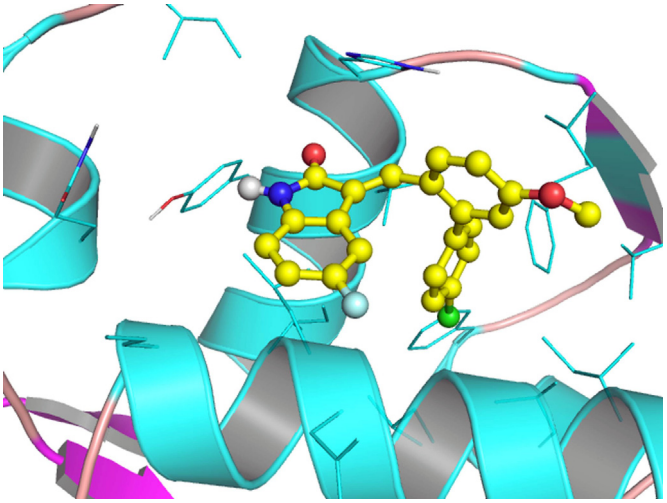

Fig. 7. Proposed binding mode of compound **2h** to MDM2 (generated using PyMol).

As shown in Table 3, compound **1b** effectively inhibited tumour growth in a dose-dependent manner, with a tumour growth inhibition (TGI) of 18.1% and 32.4% for the low and high-dose group, respectively. The TGIs observed for compound **1b** were inferior to those for the positive control, oxaliplatin, but were superior to oxaliplatin in terms of drug tolerance, as determined by the difference in body weight before and after treatment. The body weight of the oxaliplatin group decreased by 4.01 g, whereas it only decreased by 1.02 and 0.74 g for the high- and low-dose group of **1b**, respectively.

3. Conclusion

In this study, an integrated virtual screening strategy combining both pharmacophore- and structure-based approaches identified a hit compound with a (*E*)-3-benzylideneindolin-2-one scaffold as novel inhibitor of the MDM2–p53 interaction. Further optimisation led to several derivatives with potent inhibitory activity, among which **1b** showed both the highest binding affinity to MDM2 and the most potent antiproliferative activity against HCT116 (wild type p53). Additionally, it possesses a K_i value of 0.093 μM with only 21 non-hydrogen atoms, which means it possesses the highest ligand efficiency value (LE = 1.4 $pIC_{50}/N_{\text{non-hydrogen atoms}}$) [25,26] among all the synthesised compounds. Consequently, compound **1b** represents promising lead compound for the development of novel anticancer drugs as MDM2–p53 inhibitors and shows potential for optimisation to improve its activity without sacrificing its druggability. The detailed structural optimisation based on its binding mode to MDM2 proposed in this work is being carried out in our laboratory.

4. Experimental section

4.1. Synthesis and characterisation

^1H and ^{13}C NMR spectra were recorded using TMS as the internal standard in DMSO-d_6 or $CDCl_3$ with a Bruker BioSpin GmbH

Table 2
In vitro antiproliferative activity of the synthesised compounds.

Compounds	GI_{50} (μM)[a]			
	HCT116 (p53 +/+)	HCT116 (p53 −/−)	A549	MCF7
1b	13.42 ± 2.54	28.14 ± 5.0	52.50 ± 7.70	54.13 ± 7.52
2b	49.19 ± 2.82	126.3 ± 33.94	>100	>100
3b	26.94 ± 3.92	65.55 ± 3.13	>100	88.41 ± 6.44
4b	14.39 ± 1.49	21.32 ± 2.99	42.41 ± 5.60	54.01 ± 2.44
5b	20.96 ± 2.73	26.14 ± 2.67	30.19 ± 6.80	58.42 ± 11.0
6b	29.67 ± 1.58	37.72 ± 1.77	42.58 ± 4.51	55.7 ± 2.32
7b	23.40 ± 0.43	41.97 ± 1.98	30.43 ± 2.62	42.92 ± 1.71
1f	27.10 ± 1.21	124.3 ± 34.66	>100	>100
2f	17.05 ± 1.64	108.9 ± 11.78	>100	>100
3f	48.31 ± 2.76	109.9 ± 4.43	81.58 ± 13.74	>100
1h	32.19 ± 3.82	135.1 ± 49.14	86.67 ± 13.05	>100
2h	15.31 ± 1.18	27.28 ± 1.56	58.82 ± 18.82	>100
1g	53.36 ± 5.97	115.1 ± 49.14	>100	>100
Nutlin-3a	32.11 ± 3.37	55.70 ± 4.66	47.59 ± 4.53	48.74 ± 3.54

[a] The antiproliferative activity of each compound was tested by MTT assay. The GI_{50} values were indicated as mean calculated from three independent experiments. The drug exposure time was 48 h.

spectrometer at 400 and 600 MHz, respectively. The mass spectra (MS) were recorded on a Thermo Scientific LTQ ORBITRAP instrument with an ESI mass selective detector. Melting points (m.p.) were determined using an SRS-OptiMelt automated melting point instrument, without correction. Flash column chromatography was performed with silica gel (200–300 mesh) purchased from Qingdao Haiyang Chemical Co. Ltd.

*4.1.1. General procedure A for the preparation of **1a–3a***

2, 4-Dihydroxybenzaldehyde (200 mmol) and alkylation agent (440 mmol) were dissolved in 200 ml anhydrous DMF, and potassium carbonate (600 mmol) was added. The mixture was heated at 85 °C for 3.5 h, and TLC analysis indicated that the reaction was complete. The mixture was filtered, and the filtrate was concentrated *in vacuo*. The resulting residue was slowly dissolved in ethyl acetate, and was rapidly washed with distilled water. The organic layer was then dried over anhydrous $MgSO_4$ for 2 h and evaporated. The residue was recrystallised using anhydrous ethanol to give the corresponding product.

*4.1.1.1. 2,4-Dimethoxy-benzaldehyde (**1a**).* 2, 4-Dihydroxybenzaldehyde and Methyl iodide were dissolved in DMF, and the mixture was treated with K_2CO_3 according to general procedure A to afford the target compound as a white solid with the following characteristics: 95% yield; m.p. 69.1–71.2 °C; ^{1}H NMR (600 MHz, DMSO-d_6): δ 10.16 (s, 1H), 7.64 (d, J = 8.4 Hz, 1H), 6.66 (d, J = 2.4 Hz, 1H), 6.62 (dd, J = 2.4 Hz, 8.4 Hz, 1H), 3.89 (s, 3H), 3.86 (s, 3H); MS (ESI): $[M + H]^+$ m/z 167.1.

*4.1.2. 2,4-Dipropoxy-benzaldehyde (**2a**)*

2, 4-Dihydroxybenzaldehyde and 1-bromopropane were dissolved in DMF, and the mixture was treated with K_2CO_3 according to general procedure A to afford the target compound as a pale yellow solid with the following characteristics: 90% yield; ^{1}H NMR (600 MHz, DMSO-d_6): δ 10.33 (s, 1H), 7.79 (d, J = 9.0 Hz, 1H), 7.12 (dd, J = 1.8 Hz, 9.0 Hz, 1H), 6.42 (d, J = 1.8 Hz, 1H), 3.96–4.01 (m, 4H), 1.80–1.88 (m, 4H), 1.03–1.07 (m, 6H); MS (ESI): $[M + H]^+$ m/z 223.3.

*4.1.2.1. 2, 4-Diisopropoxy-benzaldehyde (**3a**).* 2, 4-Dihydroxybenzaldehyde and 2-bromopropane were dissolved in DMF, and the mixture was treated with K_2CO_3 according to general procedure A to afford the target compounds as a colourless oil with the following characteristics: 90% yield; ^{1}H NMR (600 MHz, DMSO-d_6): δ 10.17 (s, 1H), 7.61 (d, J = 8.4 Hz, 1H), 6.61 (d, J = 2.4 Hz, 1H), 6.56 (dd, J = 2.4 Hz, 8.4 Hz, 1H), 4.72–4.78 (m, 2H), 1.26–1.31 (m, 12H); MS (ESI): $[M + H]^+$ m/z 223.3.

*4.1.3. General procedure B for the preparation of **1b–7b**, **1f–3f**, and **1g–2g***

Piperidine (14.4 mL) was slowly added to a suspension of indolone (70 mmol) and substituted aldehyde (84 mmol) in 80 mL ethanol. The mixture was heated under reflux for 1.5 h, and TLC analysis indicated when the reaction was complete. After concentration *in vacuo*, the resulting residue was redissolved in ethyl acetate. Next, the mixture was successively washed with water and brine. The organic layer was dried over anhydrous $MgSO_4$, filtered and concentrated, and the resulting residue was recrystallised from anhydrous ethanol to give the corresponding product.

*4.1.3.1. 3-(2,4-Dimethoxy-benzylidene)-1,3-dihydro-indol-2-one (**1b**).* 2,4-Dimethoxy-benzaldehyde and 1,3-dihydro-indol-2-one were dissolved in ethanol, and the mixture was treated with piperidine, according to general procedure B to afford (**1b**) as a yellow solid with the following characteristics: 88% yield; m.p. 206.4–208.1 °C; ^{1}H NMR (600 MHz, $CDCl_3$): δ 7.95 (s, 1H), 7.73(d, J = 8.4 Hz, 1H), 7.66 (d, J = 8.4 Hz, 1H), 7.55 (br, 1H), 7.18 (t, J = 8.4 Hz, 1H), 6.85–6.89 (m, 2H), 6.53 (dd, J = 1.8 Hz, 8.4 Hz, 1H), 6.52 (d, J = 1.8 Hz, 1H), 3.90 (s, 3H), 3.87 (s, 3H); ^{13}C NMR (100 MHz, DMSO-d_6): δ 168.93(C), 162.70(C), 159.42(C), 142.44(C), 131.71(C), 130.66(C), 129.44(CH), 125.21(CH), 121.95(CH), 121.37(CH), 120.99(CH), 115.31(C), 109.93(CH), 105.32(CH), 98.51(CH), 55.81(CH_3), 55.53(CH_3); HRMS (ESI): Calculated for $[M + H]^+$ ($C_{17}H_{16}N_1O_3$), requires m/z 282.1130, found 282.1116.

*4.1.3.2. 5-Chloro-3-(2,4-dimethoxy-benzylidene)-1,3-dihydro-indol-2-one (**2b**).* 2,4-Dimethoxy-benzaldehyde and 5-chloro-1,3-dihydro-indol-2-one were dissolved in ethanol, and the mixture was treated with piperidine according to general procedure B to afford (**2b**) as a yellow solid with the following characteristics: 86% yield; m.p. 238.3–239.6 °C; ^{1}H NMR (600 MHz, $CDCl_3$): δ 8.01 (s, 1H), 7.68 (br, 1H), 7.62 (d, J = 1.8 Hz, 1H), 7.16 (dd, J = 1.8 Hz, 8.4 Hz, 1H), 6.80 (d, J = 8.4 Hz, 1H), 6.61 (dd, J = 2.4 Hz, 8.4 Hz, 1H), 6.53 (d, J = 2.4 Hz, 1H), 3.91 (s, 3H), 3.87 (s, 3H); ^{13}C NMR (100 MHz, DMSO-d_6): δ 168.56 (C), 163.11 (C), 159.37 (C), 141.16 (CH), 133.65 (C), 130.83 (C), 128.92 (CH), 124.80 (C), 124.23 (CH), 122.80 (C), 121.21 (CH), 114.92 (CH), 111.30 (CH), 105.54 (C), 98.62 (CH), 55.80 (CH_3), 55.65 (CH_3); HRMS (ESI): Calculated for $[M + H]^+$ ($C_{17}H_{15}Cl_1N_1O_3$), requires m/z 316.0741, found 316.0738.

*4.1.3.3. 3-(2,4-Dimethoxy-benzylidene)-6-fluoro-1,3-dihydro-indol-2-one (**3b**).* 2,4-Dimethoxy-benzaldehyde and 6-fluoro-1,3-dihydro-indol-2-one were dissolved in ethanol, and the mixture was treated with piperidine according to general procedure B to afford **3b** as a yellow solid with the following characteristics: 86% yield; m.p. 226.3–227.6 °C; ^{1}H NMR (600 MHz, $CDCl_3$): δ 8.01 (s, 1H), 7.86 (br, 1H), 7.67 (d, J = 9.0 Hz, 1H), 7.37 (dd, J = 2.4 Hz, 9.0 Hz, 1H), 6.91 (d, J = 2.4 Hz, 1H), 6.79 (d, J = 8.4 Hz, 1H), 6.59 (dd, J = 2.4 Hz, 8.4 Hz, 1H), 6.52 (d, J = 2.4 Hz, 1H), 3.90 (s, 3H), 3.87 (s, 3H); ^{13}C NMR (100 MHz, DMSO-d_6): δ 168.91(C), 163.07(C), 159.55(C), 158.34(C), 138.76(C), 133.38(C), 130.75(C), 124.92(CH), 122.36(CH), 116.06(CH), 114.92(C), 110.60(CH), 105.50(CH), 98.64(CH), 97.61(CH), 55.87(CH_3), 55.66(CH_3); HRMS (ESI): Calculated for $[M + H]^+$ ($C_{17}H_{15}F_1N_1O_3$), requires m/z 300.0958, found 300.1036.

*4.1.3.4. 3-(2,4-Dipropoxy-benzylidene)-1,3-dihydro-indol-2-one (**4b**).* 2,4-Dipropoxy-benzaldehyde and 1,3-dihydro-indol-2-one were dissolved in ethanol, and the mixture was treated with

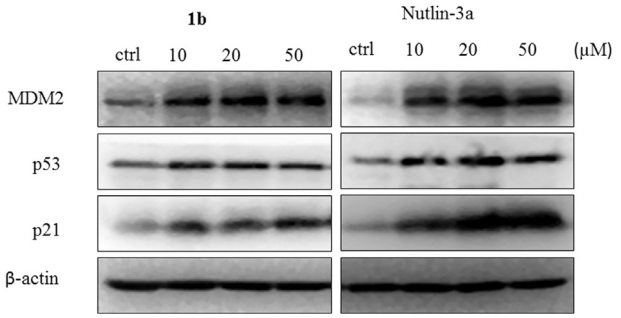

Fig. 8. The activation of the p53 pathway in HCT116 cells by compounds **1b** and nutlin-3a (western blotting).

piperidine according to general procedure B to afford **4b** as a yellow solid with the following characteristics: 86% yield; m.p. 162.3–163.4 °C; ^{1}H NMR (600 MHz, $CDCl_3$): δ 7.99 (s, 1H), 7.72 (d, J = 7.8 Hz, 1H), 7.69 (d, J = 7.8 Hz, 1H),7.18 (d, J = 8.4 Hz, 1H), 6.87 (m, 2H), 6.54 (dd, J = 2.4 Hz, 8.4 Hz, 1H), 6.50 (d, J = 2.4 Hz, 1H), 4.00 (t, J = 6.6 Hz, 2H), 3.97 (t, J = 6.6 Hz, 2H), 1.87–1.81 (m, 4H), 1.75 (t, J = 7.2 Hz, 3H), 1.02 (t, J = 7.2 Hz, 3H); ^{13}C NMR (100 MHz, DMSO-d_6): δ 168.98(C), 162.09(C), 158.85(C), 142.36(C), 131.79(C), 130.73(C), 129.35(CH), 125.04(CH), 121.93(CH), 121.44(CH), 120.94(CH), 115.34(C), 109.88(CH), 105.75(CH), 99.49(CH), 69.53(CH_3), 69.30(CH_2), 22.03(CH_2), 21.96(CH_2), 10.44(CH_3); HRMS (ESI): Calculated for $[M + H]^+$ ($C_{21}H_{23}N_1O_3$) requires m/z 338.1756, found 338.1761.

*4.1.3.5. 5-Chloro-3-(2,4-dipropoxy-benzylidene)-1,3-dihydro-indol-2-one (**5b**).* 2,4-Dipropoxy-benzaldehyde and 5-chloro-1,3-dihydro-indol-2-one were dissolved in ethanol, and the mixture was treated with piperidine according to general procedure B to afford **5b** as a yellow solid with the following characteristics: 86% yield; m.p. 171.1–172.2 °C; ^{1}H NMR (600 MHz, $CDCl_3$): δ 8.03 (s, 1H), 7.65 (d, J = 8.4 Hz, 1H), 7.63 (d, J = 2.4 Hz, 1H), 7.15 (d, J = 2.4 Hz, 8.4 Hz, 1H), 6.82(d, J = 8.4 Hz, 1H) 6.58 (dd, J = 2.4 Hz, 8.4 Hz, 1H), 6.51 (d, J = 2.4 Hz, 1H), 3.97–4.02 (m, 4H), 1.79–1.88 (m, 4H), 1.10 (t, J = 7.8 Hz, 3H), 1.02 (t, J = 7.2 Hz, 3H). ^{13}C NMR (100 MHz, DMSO-d_6): δ 168.69(C), 162.55(C), 159.00(C), 141.10(C), 133.70(C), 130.95(C), 128.80(C), 124.81(CH), 124.20(CH), 123.19(CH), 121.51(CH), 114.94(CH), 111.22(CH), 105.93(C), 99.57(CH), 69.61(CH_2), 69.40(CH_2), 22.05(CH_2), 21.94(CH_2), 10.44(CH_3); HRMS (ESI): Calculated for $[M + H]^+$ ($C_{21}H_{23}Cl_1N_1O_3$), requires m/z 372.1367, found 372.1354.

*4.1.3.6. 5-Chloro-3-(2,4-diisopropoxy-benzylidene)-1,3-dihydro-indol-2-one (**6b**).* 2,4-Dipropoxy-benzaldehyde and 5-chloro-1,3-dihydro-indol-2-one were dissolved in ethanol, and the mixture was treated with piperidine according to general procedure B to afford **6b** as a yellow solid with the following characteristics: 86% yield; m.p. 170.8–172.1 °C; ^{1}H NMR (600 MHz, $CDCl_3$): δ 8.05 (s, 1H), 8.01 (s, 1H), 7.66 (d, J = 8.4 Hz, 1H), 7.44 (d, J = 2.4 Hz, 1H), 7.13 (dd, J = 2.4 Hz, 8.4 Hz, 1H), 6.76 (d, J = 8.4 Hz, 1H) 6.52 (dd, J = 2.4 Hz, 8.4 Hz, 1H), 6.42 (d, J = 2.4 Hz, 1H), 4.58–4.67 (m, 2H), 1.40 (d, J = 6.0 Hz, 6H), 1.36 (d, J = 6.6 Hz, 6H); ^{13}C NMR: (100 MHz, DMSO-d_6): δ 168.75(C), 161.34(C), 158.09(C), 141.07(C), 134.14(C), 131.09(C), 128.73(C), 124.76(CH), 123.94(CH), 123.18(CH), 121.48(CH), 115.42(CH), 111.20(C), 106.80(CH), 101.46(CH), 70.41(CH), 69.67(CH), 21.83(CH_3); HRMS (ESI): Calculated for $[M + H]^+$ ($C_{21}H_{23}Cl_1N_1O_3$) requires m/z 372.1367, found 372.1385.

*4.1.3.7. 6-Chloro-3-(2,4-diisopropoxy-benzylidene)-1,3-dihydro-indol-2-one (**7b**).* 2,4-Diisopropoxy-benzaldehyde and 6-chloro-1,3-dihydro-indol-2-one were dissolved in ethanol, and the mixture was treated by piperidine according to general procedure B to afford **7b** as a yellow solid with the following characteristics: 86% yield; m.p. 173.1–173.9 °C; ^{1}H NMR (600 MHz, $CDCl_3$): δ 7.91 (s, 1H), 7.62 (d, J = 8.4 Hz, 1H), 7.52 (d, J = 8.4 Hz, 1H), 6.90 (dd, J = 2.4 Hz, 8.4 Hz, 1H), 6.85 (d, J = 8.4 Hz, 1H), 6.78 (dd, J = 2.4 Hz, 8.4 Hz, 1H), 6.58 (d, J = 2.4 Hz, 1H), 4.71–4.75 (m, 2H), 1.33 (d, J = 6.0 Hz, 6H), 1.28 (d, J = 6.6 Hz, 6H); ^{13}C NMR (100 MHz, DMSO-d_6): δ 169.01(C), 161.17(C), 158.08(C), 143.63(C), 133.13(C), 131.01(C), 123.59(C), 123.21(CH), 120.71(CH), 120.42(CH), 115.60(C), 109.80(CH), 106.83(CH), 101.47(CH), 70.35(CH), 69.58(CH), 21.48(CH_3); HRMS (ESI): Calculated for $[M + H]^+$ ($C_{21}H_{23}Cl_1N_1O_3$) requires m/z 372.1367, found 372.1352.

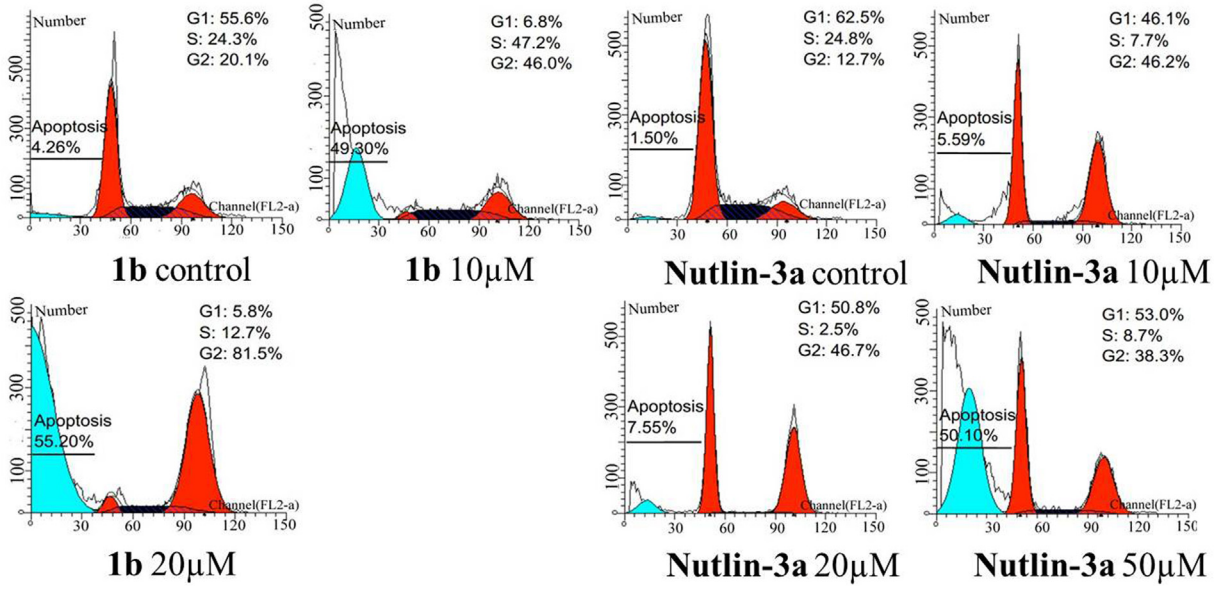

Fig. 9. G2/M phase arrest and the induction of apoptosis in HCT116 cells after treatment with compound **1b** or nutlin-3a.

Table 3
In vivo tumour growth inhibition in response to compound **1b** and oxaliplatin.

Group	Dosage (mg/kg)	No. of mice		Body weight (g)		Tumour weight[a] (g)	TGI %
		Begin	End	Begin	End		
Control	–	10	10	19.51	20.02	1.93 ± 0.39	–
Oxaliplatin	1.5	10	10	19.40	15.39	0.92 ± 0.14**	52.3
Vehicle	–	10	10	19.77	19.45	1.85 ± 0.24	4.7
1b	100	10	10	19.93	18.91	1.30 ± 0.13**	32.4
	50	10	10	19.69	18.95	1.58 ± 0.27*	18.1

[a] Student's *t*-test was used to compare the means of two groups, and analysis of variance was used to compare the means of multiple groups. For all of the differences, a P value of less than 0.05 was considered to be statistically significant.**$P < 0.01$, *$P < 0.05$.

*4.1.3.8. 2′-(5-Chloro-2-oxo-1,2-dihydro-indol-3-ylidenemethyl)-5′-methoxy-biphenyl -4-carbonitrile (**1f**).* 2′-Formyl-5′-methoxy-biphenyl-4-carbonitrile and 6-chloro-1,3-dihydro-indol-2- one were dissolved in ethanol, and the mixture was treated with piperidine according to general procedure B to afford **1f** as a yellow solid with the following characteristics: 86% yield; m.p. >280 °C; ^{1}H NMR (600 MHz, $CDCl_3$): δ 7.81 (d, J = 8.4 Hz, 2H), 7.70 (d, J = 8.4 Hz, 2H), 7.60 (s, 1H), 7.59 (d, J = 1.8 Hz, 1H), 7.46 (d, J = 8.4 Hz, 1H), 7.21 (dd, J = 1.8 Hz, 8.4 Hz, 1H), 7.07 (dd, J = 2.4 Hz, 8.4 Hz, 1H), 7.01 (d, J = 2.4 Hz, 1H), 6.82 (d, J = 8.4 Hz, 1H), 3.95 (s, 3H); ^{13}C NMR: (100 MHz, DMSO-d_6): δ 168.80(C), 168.16(C), 144.10(C), 142.23(C), 141.50(C), 136.56(C), 132.35(C), 131.19(CH), 130.84(CH), 130.52(CH), 129.39(CH), 128.19(C), 126.21(C), 124.93(CH), 124.30(CH), 122.85(CH), 121.82(CH), 118.56(CH), 115.40(C), 114.44(CH), 111.45(CH), 110.80(CH), 55.69(CH_3); HRMS (ESI): Calculated for $[M + H]^+$ ($C_{23}H_{15}Cl_1N_2O_2$) requires m/z 387.0900, found 387.0895.

*4.1.3.9. 2′-(6-Fluoro-2-oxo-1,2-dihydro-indol-3-ylidenemethyl)-5′-methoxy-biphenyl -4-carbonitrile (**2f**).* 2′-Formyl-5′-methoxy-biphenyl-4-carbonitrile and 6-fluoro-1,3-dihydro–indol -2-one were dissolved in ethanol, and the mixture was treated with piperidine according to general procedure B to afford **2f** as a yellow solid with the following characteristics: 86% yield; m.p. >280 °C; ^{1}H NMR (600 MHz, $CDCl_3$): δ 7.91 (s, 1H), 7.70 (d, J = 8.4 Hz, 2H), 7.60 (d, J = 2.4 Hz, 1H), 7.51 (d, J = 8.4 Hz, 1H), 7.46 (d, J = 8.4 Hz, 2H), 7.21 (dd, J = 2.4 Hz, 8.4 Hz, 1H), 7.07 (dd, J = 1.8 Hz, 8.4 Hz, 1H), 7.01 (d, J = 2.4 Hz, 1H), 6.82 (d, J = 8.4 Hz, 1H), 3.88 (s, 3H); ^{13}C NMR (100 MHz, DMSO-d_6): δ 168.43(C), 160.71(C), 158.39(C), 155.75(C), 144.12(C), 142.14(C), 139.07(C), 136.34(CH), 132.36(CH), 131.14(CH), 130.51(CH), 126.79(CH), 124.27(CH), 122.13(C), 118.66(CH), 116.30(CH), 116.07(C), 115.46(CH), 114.41(CH), 110.79(C), 109.53(CH), 109.26(CH), 55.68(CH_3); HRMS (ESI): Calculated for $[M + H]^+$ ($C_{23}H_{15}F_1N_2O_2$) requires m/z 371.1196, found 371.1201.

*4.1.3.10. 2′-(6-Chloro-2-oxo-1,2-dihydro-indol-3-ylidenemethyl)-6′-methoxy-biphenyl- 4-carbonitrile (**3f**).* 2′-Formyl-6′-methoxy-biphenyl-4-carbonitrile and 6-chloro-1,3-dihydro–indol -2-one were dissolved in ethanol, and the mixture was treated with piperidine according to general procedure B to afford **3f** as a yellow solid with the following characteristics: 86% yield; m.p. >280 °C; ^{1}H NMR (400 MHz, DMSO-d_6): δ 10.72 (s, 1H), 7.94 (d, J = 8.0 Hz, 2H), 7.83 (d, J = 8.0 Hz, 2H), 7.61 (d, J = 8.0 Hz, 1H), 7.42 (d, J = 2.0 Hz, 1H), 7.29–7.32 (m, 1H), 7.23 (dd, J = 2.0 Hz, 8.0 Hz, 1H), 7.17–7.19 (m, 1H), 6.90 (d, J = 8.0 Hz, 1H), 3.92 (s, 3H); ^{13}C NMR: (100 MHz, DMSO-d_6): δ 168.61(C), 166.88(C), 143.13(C), 141.50(C), 139.41(C), 136.52(C), 135.32(C), 135.07(C), 129.46(CH), 128.51(CH), 128.07(C), 124.50(CH), 124.43(CH), 122.62(CH), 122.31(CH), 121.64(CH), 113.90(C), 113.52(CH), 112.53(CH), 110.77(CH), 110.09(CH), 57.04(CH). HRMS (ESI): Calculated for $[M + H]^+$ ($C_{23}H_{15}Cl_1N_2O_2$) requires m/z 387.0900, found 387.0890.

*4.1.3.11. 3-(2-Bromo-4-methoxy-benzylidene)-5-chloro-1,3-dihydro-indol-2-one (**1g**).* 2-Bromo-4-methoxy-benzaldehyde and 6-chloro-1,3-dihydro–indol-2-one were dissolved in ethanol, and the mixture was treated with piperidine according to general procedure B to afford **1g** as a yellow solid with the following characteristics: 74% yield; m.p. 247.5–249.2 °C; ^{1}H NMR (600 MHz, $CDCl_3$): δ 7.82 (s, 1H), 7.70 (br, 1H), 7.65 (d, J = 8.4 Hz, 1H), 7.41 (d, J = 2.4 Hz, 1H), 7.25–7.26 (m, 1H), 7.18 (d, J = 2.4 Hz, 1H), 6.97 (dd, J = 2.4 Hz, 8.4 Hz, 1H), 6.81 (d, J = 8.4 Hz, 1H), 3.89 (s, 3H); ^{13}C NMR (100 MHz, DMSO-d_6): δ 168.07(C), 161.26(C), 141.73(C), 135.65(C), 131.40(C), 129.83(C), 126.95(C), 126.02(CH), 125.05(CH), 124.93(CH), 122.36(CH), 121.82(C), 118.22(CH), 114.23(CH), 111.66(CH), 56.02(CH_3); HRMS (ESI): Calculated for $[M + H]^+$ ($C_{16}H_{12}Br_1Cl_1N_1O_2$) requires m/z 363.9740, found 363.9725.

*4.1.3.12. 3-(2-Bromo-4-methoxy-benzylidene)-5-fluoro-1,3-dihydro-indol-2-one (**2g**).* 2-Bromo-4-methoxy-benzaldehyde and 5-fluoro-1,3-dihydro-indol-2-one were dissolved in ethanol, and the mixture was treated with piperidine according to general procedure B to afford **2g** as a yellow solid with the following characteristics: 92% yield; m.p. 273.7–274.2 °C; ^{1}H NMR (600 MHz, $CDCl_3$): δ 7.84 (s, 1H), 7.65 (d, J = 8.4 Hz, 1H), 7.41 (d, J = 1.8 Hz, 1H), 7.30 (d, J = 8.4 Hz, 1H), 7.19 (dd, J = 1.8 Hz, 8.4 Hz, 1H), 6.97 (dd, J = 2.4 Hz, 8.4 Hz, 1H), 6.80 (d, J = 2.4 Hz, 1H), 3.88 (s, 3H); ^{13}C NMR (100 MHz, DMSO-d_6): δ 168.61(C), 156.60(C), 144.91(C), 136.52(C), 135.07(C), 129.46(C), 128.51(C), 124.50(CH), 124.43(CH), 122.62(CH), 122.31(CH), 121.64(C), 113.52(CH), 112.53(CH), 110.09(CH), 57.04(CH_3); MS (ESI): $[M + H]^+$ m/z 350.0.

*4.1.4. General procedure C of preparation of **1d** and **2d***

Substituted bromobenzene (80 mmol), bis(pinacolato)diboron (120 mmol), potassium acetate (160 mmol) and triphenylphosphine palladium (8 mmol) were dissolved in anhydrous DMSO under N_2 protection. The mixture was heated to 85 °C for 4 h, and TLC analysis indicated when the reaction was complete. Next, distilled water was added. The mixture was extracted by ethyl acetate, dried over anhydrous $MgSO_4$ for 2 h and evaporated. The residue was chromatographed on silica gel and eluted with Petroleum ether/Ethyl acetate to produce **1d** and **2d**.

*4.1.4.1. 2-(4-Chloro-phenyl)-4,4,5,5-tetramethyl-[1,3,2]dioxaborolane (**1d**).* 1-Bromo-4-chloro-benzene was treated with bis(pinacolato)diboron according to general procedure C to afford **1d** as a white solid with the following characteristics: 60% yield; m.p. 50.1–51.1 °C; ^{1}H NMR (600 MHz, DMSO-d_6): δ 7.68 (d, J = 8.4 Hz, 2H), 7.46 (d, J = 8.4 Hz, 2H), 1.28 (s, 12H); MS (ESI): $[M + H]^+$ m/z 239.1.

*4.1.4.2. 4-(4,4,5,5-Tetramethyl-[1,3,2]dioxaborolan-2-yl)-benzonitrile (**2d**).* The 4-bromo-benzonitrile was treated with bis(pinacolato) diboron according to general procedure C to afford **2d** as a white solid with the following characteristics: 74% yield; m.p. 93.5–94.3 °C; ^{1}H NMR (400 MHz, DMSO-d_6): δ 7.66 (d, J = 8.4 Hz, 2H), 7.43 (d, J = 8.4 Hz, 2H), 1.30 (s, 12H); MS (ESI): $[M + H]^+$ m/z 230.1.

*4.1.4.3. 2′-Formyl-5′-methoxy-biphenyl-4-carbonitrile (**1e**).* Caesium carbonate (350 mmol) was added to a stirred suspension of **1d** (150 mmol) and 2-bromo-4-methoxy–benzaldehyde (150 mmol) in 100 mL DMF, followed by the addition of triphenylphosphine palladium (15 mmol). The reaction was heated at 120 °C for 4 h and then allowed to cool to room temperature. The organic solvent was removed *in vacuo* and diluted in ethyl acetate.

The entire mixture was washed with ice water (200 mL). The organic layer was then dried over anhydrous $MgSO_4$. The organic solvent was removed by rotary evaporation, and the residue was purified using column chromatography with petroleum ether/ethyl acetate to afford **1e** with the following characteristics: 70% yield; m.p. 138.7–139.9 °C; ^{1}H NMR (600 MHz, $CDCl_3$): δ 10.21 (s, 1H), 7.83 (d, J = 9.0 Hz, 2H), 7.50 (d, J = 9.0 Hz, 2H), 7.38 (d, J = 2.4 Hz, 1H), 6.77 (dd, J = 2.4 Hz, 9.0 Hz, 1H), 6.64 (d, J = 9.0 Hz, 1H), 3.84 (s, 3H); MS (ESI): $[M + H]^+$ m/z 238.1.

*4.1.4.4. 2′-Formyl-6′-methoxy-biphenyl-4-carbonitrile (**2e**).* Caesium carbonate (350 mmol) was added to a stirred suspension of **1d** (150 mmol) and 2-bromo-3-methoxy-benzaldehyde (150 mmol) in 100 mL DMF, followed by the addition of triphenylphosphine palladium (15 mmol). The reaction was heated at 120 °C for 5.5 h and then allowed to cool to room temperature. The organic solvent was removed *in vacuo* and diluted in ethyl acetate. The entire mixture was washed with ice water (200 mL). The organic layer was then dried over anhydrous $MgSO_4$. The organic solvent was removed by rotary evaporation, and the residue was purified using column chromatography with petroleum ether/ethyl acetate to afford **1e** with the following characteristics: 55% yield; m.p. 132.7–134.2 °C; ^{1}H NMR (600 MHz, DMSO-d_6): δ 9.61 (s, 1H), 7.90 (d, J = 7.8 Hz, 2H), 7.60 (t, J = 7.8 Hz, 1H), 7.52 (d, J = 7.8 Hz, 2H), 7.46 (d, J = 7.8 Hz, 2H), 3.75 (s, 3H); MS (ESI): $[M + H]^+$ m/z 238.1.

*4.1.5. General procedure C for the preparation of **1h** and **2h***

Caesium carbonate (300 mmol) was added to a stirred suspension of **1g** or **2g** (100 mmol) and **1d** in 100 mL DMF, followed by the addition of triphenylphosphine palladium (10 mmol). The reaction was heated at 120 °C for 4 h and then allowed to cool to room temperature. The organic solvent was removed *in vacuo* and diluted in ethyl acetate. The entire mixture was washed with ice water (200 mL). The organic layer was then dried over anhydrous $MgSO_4$. The organic solvent was removed by rotary evaporation, and the residue was purified using column chromatography with petroleum ether/ethyl acetate to produce **1h** and **2h**.

*4.1.5.1. 5-Chloro-3-(4′-chloro-5-methoxy-biphenyl-2-ylmethylene)-1,3-dihydro-indol-2-one (**1h**).* **1g** and **1d** were dissolved in DMF, according to general procedure C to afford compound **1h** with the following characteristics: 54% yield; m.p. 202.6–204.1 °C; ^{1}H NMR (600 MHz, $CDCl_3$): δ 7.80 (d, J = 8.4 Hz, 1H), 7.69 (d, J = 8.4 Hz, 1H), 7.60 (d, J = 3.0 Hz, 1H), 7.45 (d, J = 8.4 Hz, 2H), 7.20–7.22 (m, 1H), 7.07 (d, J = 3.0 Hz, 1H), 7.01 (dd, J = 3.0 Hz, 9.0 Hz, 1H), 6.81 (d, J = 9.0 Hz, 1H), 3.95 (s, 3H); ^{13}C NMR (100 MHz, DMSO-d_6): δ 168.08(C), 160.74(C), 144.05(C), 142.15(C), 141.46(C), 136.47(C), 132.26(C), 131.11(CH), 130.45(CH), 129.32(C), 126.20(C), 124.89(CH), 124.27(CH), 122.80(CH), 121.78(CH), 118.57(CH), 115.35(CH), 114.38(CH), 111.38(CH), 110.75(CH), 55.62(CH_3); HRMS (ESI): Calculated for $[M + H]^+$ ($C_{22}H_{15}N_1O_2Cl_2$) requires m/z 395.0480, found 395.0429.

*4.1.5.2. 3-(4′-Chloro-5-methoxy-biphenyl-2-ylmethylene)-5-fluoro-1,3-dihydro-indol-2-one (**2h**).* **2g** and **1d** were dissolved in DMF according to general procedure C to afford compound **(2h)** with the following characteristics: 65% yield; m.p. 268.2–269.7 °C; ^{1}H NMR (600 MHz, $CDCl_3$): δ 7.79 (s, 1H), 7. 78 (d, J = 8.4 Hz, 2H), 7.37 (d, J = 8.4 Hz, 2H), 7.27 (d, J = 9.0 Hz, 1H), 7.26 (s, 1H) 7.02 (d, J = 9.0 Hz, 1H), 6.93 (d, J = 8.4 Hz, 1H), 6.92 (d, J = 2.4 Hz, 1H), 6.82 (dd, J = 2.4 Hz, 8.4 Hz, 1H) 3.92 (s, 3H); ^{13}C NMR (100 MHz, DMSO-d_6): δ 168.09(C), 160.74(C), 144.06(C), 142.16(C), 141.47(C), 136.47(C), 132.26(C), 131.11(CH), 130.44(CH), 129.32(CH), 126.21(C), 124.88(CH), 124.28(CH), 122.80(C), 121.79(CH), 118.58(CH), 115.36(CH), 114.38(CH), 111.38(CH), 110.76(CH), 55.63(CH_3); HRMS (ESI): Calculated for $[M + H]^+$ ($C_{22}H_{15}N_1O_2Cl_1F_1$) requires m/z 380.0775, found 380.0849.

4.2. Biological assay

A549, HCT116 and MCF7 cell lines were purchased from the American Type Culture Collection. MDM2 binding domain (1–118) was purchased from Creative Biomart, and the PMDM-F was obtained from AnaSpec Inc. The positive control drug, nutlin-3a, was purchased from Haoyuan Chempress Shanghai. All the tested compounds were dissolved in DMSO to 100 mM stock solutions, and they were further diluted with culture medium prior to use.

4.2.1. MTT assay

The cells were seeded into a 96-well plate at a density of 5000 (100 μL) per well for 24 h, followed by drug treatment (100 μL) for 48 h. Next, 20 μL of 5 mg/ml MTT was added to the medium, and the cells were incubated for 4 h at 37 °C and 5% CO_2. After removing the culture medium, 150 μL of DMSO was added. The plates were read using an enzyme-linked immunosorbent assay plate reader at 570 nm. The viability of untreated cells was set as 100%, and the viability in the other groups was calculated by comparing the optical density reading with the control. The GI_{50} values were calculated using nonlinear regression analysis. The assays were repeated three times.

4.2.2. MDM2 binding assay

The dose-dependent binding experiments were carried out with serial dilution in DMSO of compounds. A 3 μL sample of the tested compounds and preincubated (for 30 min) MDM2 binding domain (1–118) (30 nM) and PMDM-F peptide (10 nM) in the assay buffer (100 mM potassium phosphate, pH 7.5; 100 mg/mL bovine gamma globulin; 0.02% sodium azide) was added into black 96-well microplates with F-bottom and chimney wells (Corning) to produce a final volume of 115 μL. For each assay, the controls included the MDM2 binding domain and PMDM-F. The polarisation values were measured at room temperature using Biotek Synergy H2 with a 485 nm excitation filter, a 528 nm static and polarised filter. The K_i value was calculated according to a reported method [27].

4.2.3. Western blotting

HCT116 cells (wild type p53) were treated with various concentrations of the indicated compound for 48 h. Next, the cells were harvested by centrifugation at 1000 g for 5 min. The cell pellets were washed with PBS, resuspended in lysis buffer (150 mM NaCl, 50 mM Tris (pH 8.0), 0.02% NaN_3, 0.01% PMSF, 0.2% Aprotinin, and 1% TritonX-100, supplemented with protease inhibitor cocktail (Thermo Scientific)), and centrifuged at 12,000 g for 10 min. The total protein concentration was determined using the Bio-Rad protein assay. The proteins were resolved by SDS-PAGE and transferred to a polyvinylidene fluoride membrane. After blocking with 5% non-fat milk in blocking buffer (PBS containing 0.1% Tween 20, pH 7.5), the membrane was incubated with the indicated primary antibody for 2 h at room temperature and then incubated with the appropriate peroxidase-conjugated secondary antibody. The immunoreactive bands were visualised using the ECL Plus Western Blotting Detection System (Piscataway, New Jersey, USA). Beta-actin was used as a loading control.

4.2.4. Cell cycle analysis

HCT116 cells were seeded at 2×10^5 cells/well in 6-well plates and cultured for 48 h. Next, the cells were incubated with the test compounds for 48 h. The cells were then treated with cold PBS. After harvest, the cells were fixed in 70% ice-cold ethanol overnight. Subsequently, the cells were centrifuged (1200 rpm for 5 min), the

supernatant was discarded and the pellet was treated with RNase A (100 μg/ml) for 30 min at room temperature. The cells were stained using propidium iodide at a final concentration of 50 μg/mL. The stained cells were then analysed for cell cycle distribution using flow cytometry (BECKMAN), and the changes in the cell cycle profiles was analysed using CELL QUEST PRO.

4.3. In vivo antitumour assay

Oxaliplatin was obtained from the Cancer Institute and Hospital, Chinese Academy of Medical Sciences (CAMS). BALB/mice were obtained from the Institute for Experimental Animals, Chinese Academy of Medical Sciences & Peking Union Medical College, and animal care was in compliance with the regulations issued by the Beijing Committee of Laboratory Animals.

4.3.1. Exploration of maximum administration dosage

BALB/c mice were randomised into two groups (10 mice/group), and each group was administered compound **1b** dissolved in 10% DMSO via an intraperitoneal injection at doses of 500 mg/kg and 1000 mg/kg, respectively. The mice were monitored for visible signs of toxicity for 8 days.

4.3.2. Antitumour efficiency assay

CT26 cancer cell suspensions were subcutaneously implanted into the right axilla region of the mice. Next, the BALB/c mice were randomised into 5 groups (10 mice/group) that received the following treatments: blank control, 100 mg/kg or 50 mg/kg of **1b**, 1.5 mg/kg of the positive control oxaliplatin or vehicle. The treatment was initiated 24 h after tumour implantation, and the treatments were administered once per day for ten days. Twenty-four hours after the final administration, the mice were weighed and sacrificed, and the tumours were excised, weighed and recorded for analysis.

4.4. Computational protocol

The pharmacophore was generated manually in Discovery studio 3.0 using the crystal structure of Pip-1 complexed with MDM2 (PDB ID: 2 LZG) as reference and was validated by calculating the ROC curve of the test set. Virtual screening was performed in the "screen library" module, the "conformation generation" was set to "fast", and the other parameters were set as default. The obtained compounds were further filtered by the "Rule of five", and they were then subjected to docking analysis using sybyl 7.3. The crystal structure with PDB ID 3LBL was prepared in sybyl 7.3 by removing the ligand and the water molecules and adding hydrogen atoms. The docking parameters were all set as default. After the docking was completed, a visual inspection for potential hit compounds was performed to identify the top 200 compounds ranked by docking score.

The binding mode for compounds **4b**, **1b** and **2h** were generated by molecular docking using Autodock 4.2. The receptor and the ligands were prepared using AutoDockTools and saved as pdbqt files. The centre of grid box was set to "−33.547, 16.037, −51.308", and the number of points in the *x*, *y* and *z* dimensions were 46, 48 and 44, respectively. All the parameters for docking were set as default. After docking was completed, PyMol was used to analyse the docking poses and generate publication quality figures.

Acknowledgements

This work was supported by the Central Public-interest Scientific Institution Basal Research Fund (2012IMBF05) and the National Mega-project for Innovative Drugs (2012ZX09301002-001-017).

Appendix A. Supplementary data

Supplementary data related to this article can be found at http://dx.doi.org/10.1016/j.ejmech.2014.05.027.

References

[1] J.G. Teodoro, S.K. Evans, M.R. Green, Inhibition of tumor angiogenesis by p53: a new role for the guardian of the genome, J. Mol. Med. 85 (2007) 1175–1186.
[2] J.S. Fridman, S.W. Lowe, Control of apoptosis by p53, Oncogene 22 (2003) 9030–9040.
[3] S. Shangary, S. Wang, Targeting the MDM2-p53 interaction for cancer therapy, Clin. Cancer. Res. 14 (2008) 5318–5324.
[4] A. Mullard, Protein-protein interaction inhibitors get into the groove, Nat. Rev. Drug. Discov 11 (2012) 173–175.
[5] P. Buchwald, Small-molecule protein-protein interaction inhibitors: therapeutic potential in light of molecular size, chemical space, and ligand binding efficiency considerations, IUBMB Life 62 (2010) 724–731.
[6] J. Lin, J. Chen, B. Elenbaas, A.J. Levine, Several hydrophobic amino acids in the p53 amino-terminal domain are required for transcriptional activation, binding to mdm-2 and the adenovirus 5 E1B 55-kD protein, Genes Dev. 8 (1994) 1235–1246.
[7] L.T. Vassilev, B.T. Vu, B. Graves, D. Carvajal, F. Podlaski, Z. Filipovic, N. Kong, U. Kammlott, C. Lukacs, C. Klein, N. Fotouhi, E.A. Liu, In vivo activation of the p53 pathway by small-molecule antagonists of MDM2, Science 303 (2004) 844–848.
[8] B.L. Grasberger, T. Lu, C. Schubert, D.J. Parks, T.E. Carver, H.K. Koblish, M.D. Cummings, L.V. LaFrance, K.L. Milkiewicz, R.R. Calvo, D. Maguire, J. Lattanze, C.F. Franks, S. Zhao, K. Ramachandren, G.R. Bylebyl, M. Zhang, C.L. Manthey, E.C. Petrella, M.W. Pantoliano, I.C. Deckman, J.C. Spurlino, A.C. Maroney, B.E. Tomczuk, C.J. Molloy, R.F. Bone, Discovery and cocrystal structure of benzodiazepinedione HDM2 antagonists that activate p53 in cells, J. Med. Chem. 48 (2005) 909–912.
[9] A.F. Watson, J. Liu, K. Bennaceur, C.J. Drummond, J.A. Endicott, B.T. Golding, R.J. Griffin, K. Haggerty, X. Lu, J.M. McDonnell, D.R. Newell, M.E. Noble, C.H. Revill, C. Riedinger, Q. Xu, Y. Zhao, J. Lunec, I.R. Hardcastle, MDM2-p53 protein–protein interaction inhibitors: a-ring substituted isoindolinones, Bioorg. Med. Chem. Lett. 21 (2011) 5916–5919.
[10] R. Stoll, C. Renner, S. Hansen, S. Palme, C. Klein, A. Belling, W. Zeslawski, M. Kamionka, T. Rehm, P. Mühlhahn, R. Schumacher, F. Hesse, B. Kaluza, W. Voelter, R.A. Engh, T.A. Holak, Chalcone derivatives antagonize interactions between the human oncoprotein MDM2 and p53, Biochemistry 40 (2001) 336–344.
[11] Y. Rew, D. Sun, F. Gonzalez-Lopez De Turiso, M.D. Bartberger, H.P. Beck, J. Canon, A. Chen, D. Chow, J. Deignan, B.M. Fox, D. Gustin, X. Huang, M. Jiang, X. Jiao, L. Jin, F. Kayser, D.J. Kopecky, Y. Li, M.C. Lo, A.M. Long, K. Michelsen, J.D. Oliner, T. Osgood, M. Ragains, A.Y. Saiki, S. Schneider, M. Toteva, P. Yakowec, X. Yan, Q. Ye, D. Yu, X. Zhao, J. Zhou, J.C. Medina, S.H. Olson, Structure-based design of novel inhibitors of the MDM2–p53 interaction, J. Med. Chem. 55 (2012) 4936–4954.
[12] C. Zhuang, Z. Miao, L. Zhu, G. Dong, Z. Guo, S. Wang, Y. Zhang, Y. Wu, J. Yao, C. Sheng, W. Zhang, Discovery, synthesis, and biological evaluation of orally active pyrrolidone derivatives as novel inhibitors of p53-MDM2 protein-protein interaction, J. Med. Chem. 55 (2012) 9630–9642.
[13] J.H. Lee, Q. Zhang, S. Jo, S.C. Chai, M. Oh, W. Im, H. Lu, H.S. Lim, Novel pyrrolopyrimidine-based α-Helix mimetics: cell-permeable inhibitors of protein-protein interactions, J. Am. Chem. Soc. 133 (2011) 676–679.
[14] K. Ding, Y. Lu, Z. Nikolovska-Coleska, S. Qiu, Y. Ding, W. Gao, J. Stuckey, K. Krajewski, P.P. Roller, Y. Tomita, D.A. Parrish, J.R. Deschamps, S. Wang, Structure-based design of potent non-peptide MDM2 inhibitors, J. Am. Chem. Soc. 127 (2005) 10130–10131.
[15] H.P. Beck, M. DeGraffenreid, B. Fox, J.G. Allen, Y. Rew, S. Schneider, A.Y. Saiki, D. Yu, J.D. Oliner, K. Salyers, Q. Ye, S. Olson, Improvement of the synthesis and pharmacokinetic properties of chromenotriazolopyrimidine MDM2-p53 protein-protein inhibitors, Bioorg. Med. Chem. Lett. 21 (2011) 2752–2755.
[16] M. Leão, C. Pereira, A. Bisio, Y. Ciribilli, A.M. Paiva, N. Machado, A. Palmeira, M.X. Fernandes, E. Sousa, M. Pinto, A. Inga, L. Saraiva, Discovery of a new small-molecule inhibitor of p53–MDM2 interaction using a yeast-based approach, Biochem. Pharmacol. 85 (2013) 1234–1245.
[17] G. Sarek, S. Kurki, J. Enbäck, G. Iotzova, J. Haas, P. Laakkonen, M. Laiho, P.M. Ojala, Reactivation of the p53 pathway as a treatment modality for KSHV-induced lymphomas, J. Clin. Invest. 117 (2007) 1019–1028.
[18] J.C. Carry, C. Garcia-Echeverria, Inhibitors of the p53/hdm2 protein-protein interaction-path to the clinic, Bioorg. Med. Chem. Lett. 23 (2013) 2480–2485.
[19] S. Yu, D. Qin, S. Shangary, J. Chen, G. Wang, K. Ding, D. McEachern, S. Qiu, Z. Nikolovska-Coleska, R. Miller, S. Kang, D. Yang, S. Wang, Potent and orally active small-molecule inhibitors of the MDM2-p53 interaction, J. Med. Chem. 52 (2009) 7970–7973.
[20] Y. Lu, Z. Nikolovska-Coleska, X. Fang, W. Gao, S. Shangary, S. Qiu, D. Qin, S. Wang, Discovery of a nanomolar inhibitor of the human murine double minute 2 (MDM2)-p53 interaction through an integrated, virtual database screening strategy, J. Med. Chem. 49 (2006) 3759–3962.

[21] Z. Liu, B. Li, X. Li, L. Zhang, L. Lai, Identification of small-molecule inhibitors against human leukocyte antigen-death receptor 4 (HLA-DR4) through a comprehensive strategy, J. Chem. Inf. Model. 51 (2011) 326–334.
[22] I. Wallach, R. Lilien, Virtual decoy sets for molecular docking benchmarks, J. Chem. Inf. Model. 51 (2011) 196–202.
[23] S.F. Sousa, P.A. Fernandes, M.J. Ramos, Protein-ligand docking: current status and future challenges, Proteins 65 (2006) 15–26.
[24] Z. Xu, Z. Liu, T. Chen, T. Chen, Z. Wang, G. Tian, J. Shi, X. Wang, Y. Lu, X. Yan, G. Wang, H. Jiang, K. Chen, S. Wang, Y. Xu, J. Shen, W. Zhu, Utilization of halogen bond in lead optimization: a case study of rational design of potent phosphodiesterase type 5 (PDE5) inhibitors, J. Med. Chem. 15 (2011) 5607–5611.
[25] M.D. Shultz, Setting expectations in molecular optimizations: strengths and limitations of commonly used composite parameters, Bioorg. Med. Chem. Lett. 23 (2013) 5980–5991.
[26] A.L. Hopkins, C.R. Grooml, A. Alex, Ligand efficiency: a useful metric for lead selection, Drug. Discov. Today 9 (2004) 430–431.
[27] Z. Nikolovska-Coleska, R. Wang, X. Fang, H. Pan, Y. Tomita, P. Li, P.P. Roller, K. Krajewski, N.G. Saito, J.A. Stuckey, S. Wang, Development and optimization of a binding assay for the XIAP BIR3 domain using fluorescence polarization, Anal. Biochem. 332 (2004) 261–273.